Steady viscoelastic fluid flow between parallel plates under electro-osmotic forces: Phan-Thien–Tanner model

S. Dhinakaran [a], A.M. Afonso [a], M.A. Alves [a], F.T. Pinho [b,*]

[a] CEFT, Departamento de Engenharia Química, Faculdade de Engenharia da Universidade do Porto, Rua Dr. Robert Frias, 4200-465 Porto, Portugal
[b] CEFT, Departamento de Engenharia Mecânica, Faculdade de Engenharia da Universidade do Porto, Rua Dr. Robert Frias, 4200-465 Porto, Portugal

ABSTRACT

The electro-osmotic flow of a viscoelastic fluid between parallel plates is investigated analytically. The rheology of the fluid is described by the Phan-Thien–Tanner model. This model uses the Gordon–Schowalter convected derivative, which leads to a non-zero second normal stress difference in pure shear flow. A nonlinear Poisson–Boltzmann equation governing the electrical double-layer field and a body force generated by the applied electrical potential field are included in the analysis. Results are presented for the velocity and stress component profiles in the microchannel for different parametric values that characterize this flow. Equations for the critical shear rates and maximum electrical potential that can be applied to maintain a steady fully developed flow are derived and discussed.

© 2010 Elsevier Inc. All rights reserved.

1. Introduction

The theoretical analysis of electro-osmotic flows (EOF) of Newtonian fluids in microchannels has been the subject of several studies. Burgreen and Nakache [1] studied the effect of the surface potential on liquid transport through ultrafine capillary slits assuming the validity of the Debye–Hückel linear approximation to the electrical potential distribution under an imposed electrical field. Rice and Whitehead [2] discussed the same problem in a circular capillary. Dutta and Beskok [3] obtained analytical solutions for the velocity distribution, mass flow rate, pressure gradient, wall shear stress, and vorticity in mixed electro-osmotic/pressure driven flows for a two-dimensional straight channel geometry, for small, yet finite symmetric electrical double layers (EDL), relevant for applications where the distance between the two walls of a microfluidic device is about 1–3 orders of magnitude larger than the EDL thickness. Arulanandam and Li [4] and Wang et al. [5] presented a two-dimensional analytical model for the electro-osmotic flow in a rectangular microchannel. Wang et al. [6] derived a semi-analytical solution to study the flow behaviour of periodical electro-osmosis in a rectangular microchannel based on the Poisson–Boltzmann and the Navier–Stokes equations. Zade et al. [7] presented analytical solutions for the heat transfer characteristics of Newtonian fluids under combined pressure and electro-osmotic flow forcing in planar microchannels. Analytical solutions for the

two-dimensional, time-dependent as well as time-independent EOF driven by a uniform electric field with non-uniform zeta potential distributions along the walls of a conduit were presented by Qian and Bau [8]. Several other articles can be found in the literature on theoretical studies of EOF with Newtonian fluids in microchannels such as those of Petsev and Lopez [9], Qian and Bau [10], among others.

Biofluids are often solutions of long chain molecules which impart a non-Newtonian rheological behaviour characterized by variable viscosity, memory effects, normal stress effect, yield stress and hysteresis of fluid properties. These fluids are encountered in chips used for chemical and biological analysis or in micro-rheometers.

The theoretical study of electro-osmotic flows of non-Newtonian fluids is recent and has been mostly limited to simple inelastic fluid models, such as the power-law, due to the inherent analytical difficulties introduced by more complex constitutive equations. Examples are the recent works of Das and Chakraborty [11] and Chakraborty [12], who presented explicit relationships for velocity, temperature and concentration distributions in electro-osmotic microchannel flows of non-Newtonian bio-fluids described by the power-law model. Other purely viscous models were analytically investigated by Olivares et al. [13], who considered the existence of a small wall layer depleted of additives and behaving as a Newtonian fluid (the skimming layer), under the combined action of pressure and electrical fields, thus restricting the non-Newtonian behaviour to the electrically neutral region outside the electrical double layer. Very recently these studies were extended to viscoelastic fluids by Afonso et al. [14], who presented analytical

* Corresponding author. Fax: +351 22 508 1440.
   E-mail addresses: dhina@fe.up.pt (S. Dhinakaran), aafonso@fe.up.pt (A.M. Afonso), mmalves@fe.up.pt (M.A. Alves), fpinho@fe.up.pt (F.T. Pinho).

Nomenclature

De_κ	Deborah number, $\lambda\kappa u_{sh}$		ϕ	electric potential in the streamwise direction (imposed) [V]
e	elementary charge [1.6022×10^{-19} C]			
E_x	x-component of imposed electric gradient [V m^{-1}]		$\dot{\gamma}$	velocity gradient [s^{-1}]
$f(\tau_{kk})$	PTT stress coefficient function		η	polymer viscosity coefficient [Pa s]
H	half-height of the microchannel [m]		κ^2	Debye Hückel parameter [m^{-2}]
k_B	Boltzmann constant [1.3807×10^{-23} J K^{-1}]		λ	relaxation time [s]
L	microchannel length [m]		λ_D	Debye layer thickness [m]
n_0	ionic number concentration [m^{-3}]		μ	viscometric viscosity [Pa s]
t	time [s]		ρ_e	electric charge density [C m^{-3}]
T	absolute temperature [K]		τ_{xx}, τ_{yy}	normal stresses [Pa]
u	x-component of velocity [m s^{-1}]		τ_{xy}	shear stress [Pa]
u_{sh}	Helmholtz–Smoluchowski velocity [m s^{-1}]		τ_{kk}	trace of the extra stress tensor [Pa]
x	axial direction [m]		ξ	PTT model parameter that accounts for the slip between molecular network and the continuum medium
y	transverse co-ordinate [m]			
W	microchannel width [m]		ψ	potential field in the transverse direction (induced) [V]
z	valence of ions		ψ_0	wall zeta potential [V]

Tensors and vectors			*Subscripts*	
D	rate of deformation tensor [s^{-1}]		c	refers to critical value
E	external applied electric field [V m^{-1}]		κ	refers to Debye–Hückel parameter
u	velocity vector [m s^{-1}]		sh	refers to Helmholtz–Smoluchowski
τ	polymeric extra-stress tensor [Pa]		s	refers to solvent

Greek			*Superscript*	
ε	Extensibility parameter of PTT model		$\diamond$	Gordon–Schowalter convected derivative
$\in$	dielectric constant of the fluid [C V^{-1} m^{-1}]		-	dimensionless quantity

solutions for channel and pipe flows of viscoelastic fluids under the mixed influence of electro-kinetic and pressure forces, using two constitutive models: the Phan-Thien–Tanner model (PTT [15]), with linear kernel for the stress coefficient function and zero second normal stress difference [16], and the kinetic theory based Finitely Extensible Non-linear Elastic model with a Peterlin closure for the average dumbbell spring force (cf. [17]) denoted as FENE-P model. Their analysis [14] was restricted to cases with small electric double-layers, where the distance between the walls of a microfluidic device is at least one order of magnitude larger than the EDL, and the fluid is uniformly distributed across the channel.

Afonso et al. [14] also showed that when the viscoelastic flow is induced by a combination of both electric and pressure potentials, in addition to the contributions from these two isolated mechanisms there is an extra term in the velocity profile that simultaneously combines both forcings, which is absent for the Newtonian fluids where the superposition principle applies. This extra term can contribute significantly to the total flow rate, and appears only when the rheological constitutive equation is non-linear. Afonso et al. [18] extended their earlier study [14] to the flow of viscoelastic fluids under asymmetric zeta potential forcing, whereas Sousa et al. [19] considered the effect of a Newtonian skimming layer for the PTT fluid.

Flow instabilities can occur for a variety of reasons. For instance, they are associated with perturbations to non-linear terms of the governing equations which grow without control. Generally speaking, in electro-osmotic flows in microchannels, flow instabilities can be promoted by oscillating electric fields, as was justified by Boy and Storey [20] among others. They can also be promoted by gradients of conductivity as shown in the experimental study of Lin et al. [21] who also analyzed the problem theoretically and numerically.

In addition to inertial non-linearities, which require high Reynolds number flows, non-Newtonian fluids are also prone to flow instabilities due to non-linearities in their rheological behaviour.

For instance, for viscoelastic fluids constitutive instabilities in Poiseuille and Couette flows were observed when the constitutive equation exhibits a non-monotonic behaviour for the shear stress, as reported by Alves et al. [22] for the full PTT model, and by Español et al. [23] and Georgiou and Vlassopoulos [24] for the Johnson–Segalman (JS) constitutive equation [25]. To the best knowledge of the authors this constitutive instability in microchannels under EOF has not yet been studied. There are other viscoelastic flow instabilities not associated with non-monotonic fluid properties, but these are not considered here.

In this study, we extend the work of Afonso et al. [14] considering the full Gordon–Schowalter convective derivative in the PTT model to analyze the steady fully developed flow in the microchannel. We derive expressions for the critical shear rates and Deborah number beyond which constitutive flow instability occurs. The rest of the paper is organised as follows. The physical description of the problem is given in Section 2 while the equations governing the flow are presented in Section 3. The analytical solutions are derived in Section 4. Section 5 discusses the results of the study and the conclusions are presented in Section 6.

2. Physical description of the problem

The geometry under consideration is shown schematically in Fig. 1, where a microchannel is formed between two parallel plates separated by a distance (height) $2H$. The length of the channel is L and the width is W, both assumed to be much larger than the height, i.e., $L, W \gg 2H$. The bottom plate is located at $y = -H$ while the top plate is located at $y = H$. A potential is applied along the axis of the channel which provides the necessary driving force for the flow through electro-osmosis. Due to symmetry of the geometry and flow conditions with respect to the channel mid-
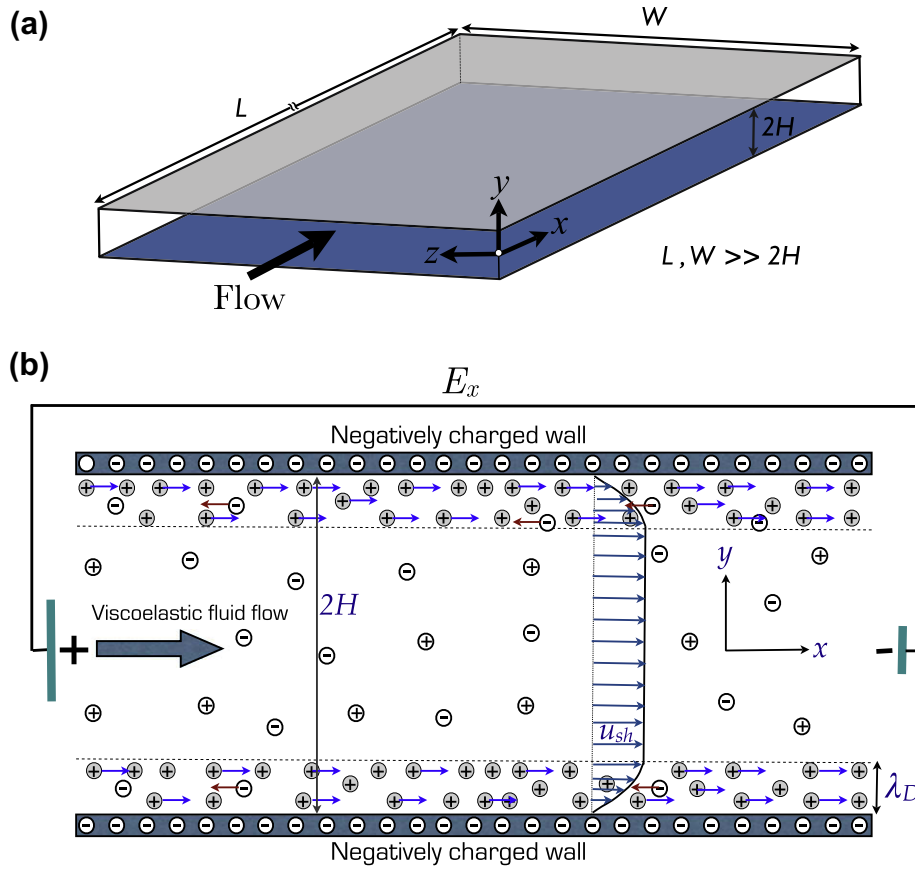
Fig. 1. (a) Diagram of the microchannel geometry considered in the study; (b) 2D representation of electro-osmotic flow of viscoelastic fluids in the microchannel for a negatively charged wall.

plane ($y = 0$), only the upper half of the channel ($0 \leqslant y \leqslant H$) is considered in this analysis.

3. Governing equations

The equations governing the flow of an incompressible fluid between the parallel walls of the microchannel are the continuity and the modified Cauchy equation,

$$\nabla \cdot \mathbf{u} = 0 \tag{1}$$

$$\rho \frac{D\mathbf{u}}{Dt} = -\nabla p + \nabla \cdot \boldsymbol{\tau} + \eta_s \nabla^2 \mathbf{u} + \mathbf{F} \tag{2}$$

where $\mathbf{u}$ is the velocity vector, t the time, ρ the fluid density, η_s is the Newtonian solvent viscosity and $\boldsymbol{\tau}$ the polymeric contribution to the extra-stress tensor. Here, we consider that the solvent viscosity is negligible in comparison with the polymeric contribution, i.e., $\eta_s = 0$. The term $\mathbf{F}$ in the modified momentum Eq. (2) represents a body force per unit volume, given by

$$\mathbf{F} = \rho_e \mathbf{E} \tag{3}$$

where $\mathbf{E} = -\nabla \phi$ is the applied external electric field and ρ_e is the net electric charge density. The potential has two contributions: (a) an applied external field, $\mathbf{E}$ and (b) a spontaneously induced potential that appears near the wall, ψ. The formation of the EDL in a fluid containing charged species occurs spontaneously when the fluid is brought in contact with the microchannel walls, causing a preferential redistribution of the charged species in the fluid and wall [26,27]. In order to obtain the induced potential field, the net charge density distribution (ρ_e) has to be solved as discussed in Section 3.2.

3.1. Constitutive equation

The model adopted here to describe the viscoelastic behaviour of the fluid is the PTT model [15], which can be expressed as

$$f(\tau_{kk})\boldsymbol{\tau} + \lambda \overset{\diamond}{\boldsymbol{\tau}} = 2\eta \mathbf{D} \tag{4}$$

where $\mathbf{D} = (\nabla \mathbf{u^T} + \nabla \mathbf{u})/2$ is the rate of deformation tensor, λ is the relaxation time, η is the polymer viscosity coefficient and $\overset{\diamond}{\boldsymbol{\tau}}$ represents the Gordon–Schowalter convected derivative of the stress-tensor, defined as

$$\overset{\diamond}{\boldsymbol{\tau}} = \frac{D\boldsymbol{\tau}}{Dt} - \nabla \mathbf{u^T} \cdot \boldsymbol{\tau} - \boldsymbol{\tau} \cdot \nabla \mathbf{u} + \xi(\boldsymbol{\tau} \cdot \mathbf{D} + \mathbf{D} \cdot \boldsymbol{\tau}) \tag{5}$$

where ε is the extensibility parameter and parameter ξ accounts for the slip between the molecular network and the continuum medium [15]. A simplified version of the above model is the so-called simplified Phan-Thien–Tanner (sPTT) equation, where $\xi = 0$. The stress coefficient function, $f(\tau_{kk})$ is given by the linear form,

$$f(\tau_{kk}) = 1 + \frac{\varepsilon \lambda}{\eta} \tau_{kk} \tag{6}$$

where $\tau_{kk} = \tau_{xx} + \tau_{yy} + \tau_{zz}$ represents the trace of the extra-stress tensor. As the flow is two dimensional, we have $\tau_{zz} = 0$. When $f(\tau_{kk}) = 1$ (i.e., when $\varepsilon = 0$, but $\xi \neq 0$), the Johnson–Segalman constitutive equation, used for dilute polymeric solutions, is recovered.

3.2. Potential field within the electric double layer

The flow investigated is steady and fully developed and in addition the electric double layers (EDLs) are thin so that there is no

interference from one wall into the other. These conditions simplify the Nernst–Planck equations governing the ionic and electric potential field (ψ) distributions. Consequently, the potential field within the electric double layer can be given by the well known Poisson equation:

$$\nabla^2 \psi = -\frac{\rho_e}{\in} \tag{7}$$

where $\in$ is the dielectric constant of the solution. We are here considering standard kinetic theory conditions, where the applied constant potential streamwise gradient ($\Delta\phi/L$, where L is the channel length) is much weaker than the induced transverse ion potential (ψ_o/λ_D) so mutual interference is negligible. The distribution of the net electric charge density, ρ_e, in equilibrium near a charged surface, as in a fully developed flow, is described as [26]

$$\rho_e = -2n_o ez \sinh\left(\frac{ez}{k_B T}\psi\right) \tag{8}$$

For small values of ψ, the Debye–Hückel linearization principle ($\sinh x \approx x$) can be used, which means physically that the electrical potential is small compared with the thermal energy of the charged species. Invoking this principle, the Poisson–Boltzmann equation resulting from substitution of Eq. (8) into Eq. (7) takes the following simpler linear form

$$\frac{d^2\psi}{dy^2} = \kappa^2 \psi \tag{9}$$

where $\kappa^2 = 2n_o e^2 z^2/(\in k_B T)$ is the Debye–Hückel parameter, related with the thickness of the Debye layer, $\lambda_D = 1/\kappa$ (normally referred as the EDL thickness). This approximation is valid when the Debye thickness is small but finite, i.e., for $10 \leqslant H/\lambda_D \leqslant 10^3$. As a consequence the induced potential is limited so that its energy does not exceed the thermal energy.

Eq. (9) can be solved subjected to the following boundary conditions: zeta potential at the wall, $\psi_{\|y=H} = \psi_0$ and symmetry in the centerline, $(d\psi/dy)_{\|y=0} = 0$, and can be written in dimensionless form as

$$\bar{\psi} = \frac{\cosh(\bar{\kappa}\bar{y})}{\cosh(\bar{\kappa})} \tag{10}$$

where the following non-dimensional quantities are defined: $\bar{\psi} = \psi/\psi_0$, $\bar{\kappa} = \kappa H$ and $\bar{y} = y/H$. Finally, the net charge density distribution Eq. (8) in conjunction with Eq. (10) reduces to

$$\rho_e = -\in \psi_0 \kappa^2 \frac{\cosh(\bar{\kappa}\bar{y})}{\cosh(\bar{\kappa})} \tag{11}$$

4. Analytical solution

4.1. PTT constitutive equation

The predictions of the PTT model in this flow, for which $\mathbf{u} = \{u(y), 0, 0\}$, can be obtained from Eqs. (4)–(6), and leads to

$$f(\tau_{kk})\tau_{xx} = \lambda(2-\xi)\dot{\gamma}\tau_{xy} \tag{12}$$
$$f(\tau_{kk})\tau_{yy} = -\lambda\xi\dot{\gamma}\tau_{xy} \tag{13}$$
$$f(\tau_{kk})\tau_{xy} = \eta\dot{\gamma} + \lambda\left(1-\frac{\xi}{2}\right)\dot{\gamma}\tau_{yy} - \frac{\lambda\xi}{2}\dot{\gamma}\tau_{xx} \tag{14}$$

where $\tau_{kk} = \tau_{xx} + \tau_{yy}$ is the trace of the extra-stress tensor and $\dot{\gamma}$ is the velocity gradient ($\dot{\gamma} = du/dy$). Upon division of Eq. (12) by Eq. (13) the specific function $f(\tau_{kk})$, $\dot{\gamma}$ and τ_{xy} cancel out, and a relation between the two normal stresses is obtained,

$$\tau_{yy} = -\frac{\xi}{2-\xi}\tau_{xx} \tag{15}$$

leading to the following form of the stress coefficient function:

$$f(\tau_{kk}) = 1 + \frac{2\varepsilon\lambda(1-\xi)}{\eta(2-\xi)}\tau_{xx} \tag{16}$$

Division of Eq. (14) by Eq. (12) results in a second order algebraic equation for the streamwise normal stress,

$$\lambda\xi\tau_{xx}^2 - \eta\tau_{xx} + \lambda(2-\xi)\tau_{xy}^2 = 0 \tag{17}$$

which leads to the following physical solution for τ_{xx} (note that at the centerline, τ_{xx} and τ_{xy} should be zero)

$$\tau_{xx} = \frac{\eta}{2\lambda\xi}\left[1 - \sqrt{1 - \frac{4\lambda^2\xi(2-\xi)}{\eta^2}\tau_{xy}^2}\right] \tag{18}$$

4.2. Analytical flow solution for the PTT model

From the invoked assumptions and for a zero pressure gradient, the momentum Eq. (2) reduces to

$$\frac{d\tau_{xy}}{dy} = -\rho_e E_x \tag{19}$$

where $E_x = -d\phi/dx$ is the streamwise gradient of the applied external electric potential (ϕ). Using Eq. (11) and noting that $\tau_{xy\|y=0} = 0$, Eq. (19) can be integrated to yield

$$\tau_{xy} = \in \psi_0 E_x \kappa \frac{\sinh(\kappa y)}{\cosh(\kappa H)} \tag{20}$$

Using the relation between the normal and shear stresses – equation (18), an explicit expression for the normal stress component is obtained,

$$\tau_{xx} = \frac{\eta}{2\lambda\xi}\left[1 - \sqrt{1 - \left(a\lambda\kappa u_{sh}\frac{\sinh(\kappa y)}{\cosh(\kappa H)}\right)^2}\right] \tag{21}$$

with a defined as $a = 2\sqrt{\xi(2-\xi)}$, for compactness and $u_{sh} = -\in \psi_o E_x/\eta$ is the Helmholtz–Smoluchowski velocity based on the zero-shear rate viscosity. After combining Eqs. (14)–(16), (20) and (21) we obtain an expression for the velocity gradient:

$$\dot{\gamma} = \frac{du}{dy} = -\frac{\left[1 + \frac{1}{\chi}\left\{1 - \sqrt{1 - \left(a\lambda\kappa u_{sh}\frac{\sinh(\kappa y)}{\cosh(\kappa H)}\right)^2}\right\}\right]\kappa u_{sh}\frac{\sinh(\kappa y)}{\cosh(\kappa H)}}{1 - \frac{1}{2}\left[1 - \sqrt{1 - \left(a\lambda\kappa u_{sh}\frac{\sinh(\kappa y)}{\cosh(\kappa H)}\right)^2}\right]} \tag{22}$$

with χ defined as $\chi = \frac{\xi(2-\xi)}{\varepsilon(1-\xi)}$, in order to improve the readability. Integrating Eq. (22) and applying the no-slip boundary condition at the wall (i.e., $u = 0$, at $y = H$) the following velocity profile is obtained:

$$u = \frac{2\cosh(\kappa H)}{a^2\lambda^2\kappa^2 u_{sh}}\left(\frac{2+\chi}{\chi}\right)\left[\frac{1}{2}\ln\left\{\frac{(1+A(H))(1-A(y))}{(1-A(H))(1+A(y))}\right\}\right.$$
$$- \ln\left\{\frac{\tanh\left(\frac{\kappa y}{2}\right)}{\tanh\left(\frac{\kappa H}{2}\right)}\right\} - \frac{1}{(2+\chi)}\frac{a^2\lambda^2\kappa^2 u_{sh}^2}{\cosh(\kappa H)}\left\{1 - \frac{\cosh(\kappa y)}{\cosh(\kappa H)}\right\}$$
$$\left. - \frac{a\lambda\kappa u_{sh}}{\cosh(\kappa H)}(\arcsin\{B\cosh(\kappa y)\} - \arcsin\{B\cosh(\kappa H)\})\right] \tag{23}$$

where,

$$A(y) = \frac{\cosh(\kappa y)}{\sqrt{1 - \left[a\lambda\kappa u_{sh}\frac{\sinh(\kappa y)}{\cosh(\kappa H)}\right]^2}}; \quad B = \frac{\frac{a\lambda\kappa u_{sh}}{\cosh(\kappa H)}}{\sqrt{1 + \left[\frac{a\lambda\kappa u_{sh}}{\cosh(\kappa H)}\right]^2}}$$

Eq. (23) can be written in dimensionless form as

$$u/u_{sh} = \frac{2}{G\,aDe_\kappa}\left(\frac{2+\chi}{\chi}\right)\left[\frac{1}{2}\ln\left\{\frac{(1+\overline{A}(1))(1-\overline{A}(\bar{y}))}{(1-\overline{A}(1))(1+\overline{A}(\bar{y}))}\right\}\right.$$
$$-\ln\left\{\frac{\tanh\left(\frac{\bar{\kappa}\bar{y}}{2}\right)}{\tanh\left(\frac{\bar{\kappa}}{2}\right)}\right\} - \frac{1}{(2+\chi)}G\,aDe_\kappa\left\{1-\frac{\cosh(\bar{\kappa}\bar{y})}{\cosh(\bar{\kappa})}\right\}$$
$$\left.-G\left(\arcsin\{\overline{B}\cosh(\bar{\kappa}\bar{y})\} - \arcsin\{\overline{B}\cosh(\bar{\kappa})\}\right)\right] \qquad (24)$$

with the dimensionless forms of A and B,

$$\overline{A}(\bar{y}) = \frac{\cosh(\bar{\kappa}\bar{y})}{\sqrt{1-G^2\sinh^2(\bar{\kappa}\bar{y})}}; \quad \overline{B} = \frac{G}{\sqrt{1+G^2}} \quad \text{and} \quad G = \frac{aDe_\kappa}{\cosh(\bar{\kappa})}$$

where $De_\kappa = \lambda\kappa u_{sh}$ is a Deborah number.

4.2.1. Critical shear rate

A physical solution for the transverse profile of velocity, in Eq. (23), only occurs when

$$\left[a\lambda\kappa u_{sh}\frac{\sinh(\kappa y)}{\cosh(\kappa H)}\right]^2 \leqslant 1$$

Thus, at critical conditions (that occurs at the wall):

$$\sinh(\kappa H) = \frac{\cosh(\kappa H)}{a\lambda\kappa|u_{sh}|} \qquad (25)$$

Substituting Eq. (25) in Eq. (22), we conclude that the critical shear rate $|\dot{\gamma}_c|$ is

$$\lambda|\dot{\gamma}_c| = \frac{\varepsilon(1-\xi)+\xi(2-\xi)}{[\xi(2-\xi)]^{3/2}} \qquad (26)$$

This is the same constitutive instability obtained by Alves et al. [22] for pressure-driven channel flows, and is related with the existence of a local maximum of the shear stress as a function of the shear rate for the PTT model without a solvent viscosity, and occurs for the condition indicated in Eq. (26), independent of the mechanism used to drive the flow [22]. This critical shear rate depends on both ε and ξ, i.e., it is a characteristic of the PTT model and independent of the type of forcing. Above the maximum shear rate given in Eq. (26), the governing equations for the flow between the walls of the microchannel do not have a real solution, and the fully-developed steady solution no longer exists.

4.2.2. Expression for critical Deborah number

Under critical conditions at the wall, multiplying Eq. (22) by λ results in the expression

$$\lambda\dot{\gamma}_c = -2\left[1+\frac{1}{\chi}\right]De_\kappa\tanh(\kappa H)$$

For $\kappa H > 10$, $\tanh(\kappa H) \to 1$ and the previous equation takes the form

$$\lambda\dot{\gamma}_c = -2\left[1+\frac{1}{\chi}\right]De_\kappa \qquad (27)$$

Equating Eq. (26) and (27) we get a relation for the critical Deborah number as

$$|De_{\kappa,c}| = \frac{1}{a} \qquad (28)$$

Beyond this critical value of $De_{\kappa,c}$ the flow cannot be steady and fully developed, as the shear rate near the wall exceeds the critical value. An expression for the corresponding critical electric potential, that can be applied, $E_{x,c}$, can be obtained from Eq. (28) and is given by

$$|E_{x,c}| = \frac{\eta}{a\lambda\kappa\in|\psi_o|} \qquad (29)$$

This expression is useful in setting the electric field along the channel so as to have a stable flow. If a strong forcing is imposed, the flow must naturally evolve to a different condition, presumably an unsteady flow. Note that an asymmetric steady flow would lead to a shear rate beyond the critical value of Eq. (26) at one of the walls, thus reinforcing the idea that only an unsteady flow is possible. However, the investigation of the flow characteristics above this critical condition and of the transition process requires the use of various different specific tools.

5. Results and discussion

The general equations for the flow of viscoelastic fluids in microchannels under the influence of electro-osmosis were derived in Section 4. The influence of electro-kinetic forcing and fluid rheology on the velocity profile has been identified in Eq. (23). Important limiting cases contained in the general solutions are: (a) Newtonian flow under the sole influence of electrokinetic forces and (b) viscoelastic fluid with zero second normal stress difference, i.e., the simplified Phan-Thien–Tanner (sPTT) equation with $\xi = 0$.

For a Newtonian fluid the relaxation time is zero and the Deborah number vanishes ($De_\kappa = \lambda\kappa u_{sh} = 0$, although also true, it suffices to impose $\lambda = 0$), so the velocity profile is only a function of the wall distance and the relative microchannel ratio, $\bar{\kappa}$, as shown earlier by Burgreen and Nakache [1]. Fig. 2 shows the effect of the relative microchannel ratio, $\bar{\kappa}$ (or H/λ_D, where λ_D is the Debye layer thickness) on the dimensionless velocity profiles (u/u_{sh}) for pure electro-osmotic flow. As $\bar{\kappa} \to 1$ the double layer thickness becomes of the same order of magnitude as the channel half-height and the region of excess charge is distributed over the entire channel. This situation is not fully compatible with this solution for which the Debye–Hückel approximation was invoked, which requires $\bar{\kappa} \geqslant 10$. As $\bar{\kappa}$ increases, the width of the Debye layer decreases, and the profile becomes sharper near the wall, as illustrated in Fig. 2.

The effect of De_κ on the dimensionless velocity profiles is shown in Fig. 3 at different Deborah numbers and fixed ε and ξ while $\bar{\kappa} = 20$. At large Deborah numbers, the ratio u/u_{sh} is significantly greater than unity near the centerline due to shear-thinning of the viscosity of the PTT fluid and the consequent lower viscosities
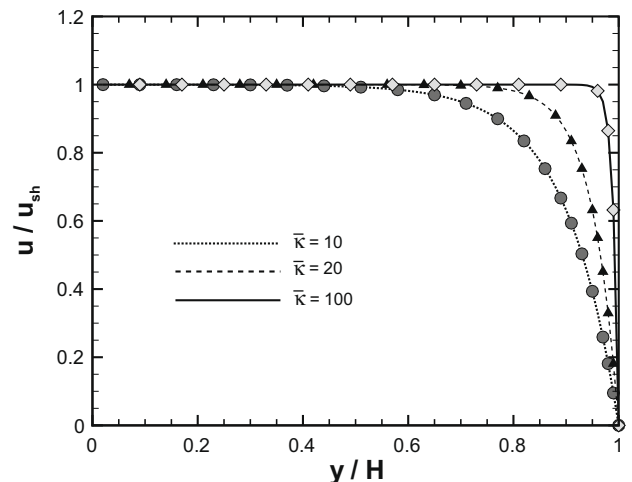
Fig. 2. Dimensionless velocity profiles for $\bar{\kappa} = 10, 20$ and 100 for pure electro-osmotic flow of a Newtonian fluid. Symbols represent the data from Burgreen and Nakache [1].
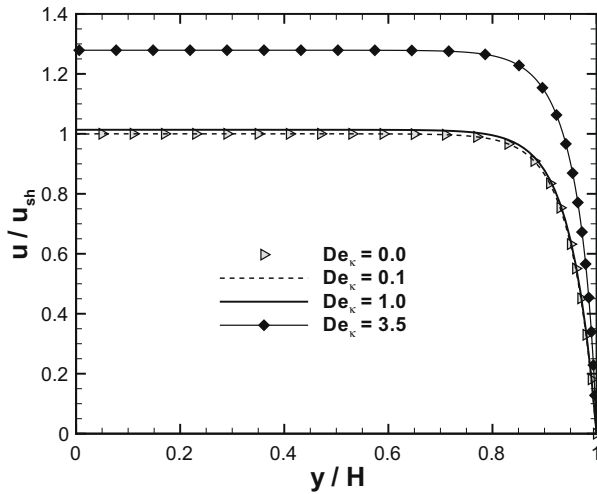
Fig. 3. Effect of $De_\kappa (\varepsilon, \xi = 0.01, \bar\kappa = 20)$ on the non-dimensional velocity profiles for the viscoelastic fluid flow in the microchannel under the influence of electro-osmotic forces.

at the wall region. With a decrease in De_κ, shear thinning effects become less important, and below $De_\kappa = 0.1$ the dimensionless velocity profile remains unaltered, and equal to the profile for a Newtonian fluid.

The flow between the parallel walls of the microchannel depends on rheological and electro-osmotic parameters. The influence of ε and ξ on the dimensionless transverse velocity profiles are plotted in Fig. 4a and b, respectively, for $\bar\kappa = 20$ at $De_\kappa = 3.0$. Upon fixing De_κ and ξ and decreasing ε from 0.2 to 0.001, we find that the dimensionless velocity profiles approach the solution for Johnson–Segalman fluid ($\varepsilon = 0$), which in this case is similar to the Newtonian solution because of the small ξ used, as seen in Fig. 4a. The variation of the non-dimensional velocity profiles at $\xi = 0.001, 0.005$ and 0.01 is presented in Fig. 4b for $De_\kappa = 3$ and $\varepsilon = 0.1$. Increasing ξ from 0.001 to 0.01 increases the velocity profile due to enhanced shear-thinning associated with ξ.

The critical Deborah number ($|De_{\kappa,c}|$), predicted from Eq. (28) is presented in Fig. 5 as a function of ξ. In log–log scale $De_{\kappa,c}$ decreases monotonically and linearly as the parameter ξ increases (with a slope of $-1/2$) for small values of ξ, and in the limiting case of $\xi = 0$ (sPTT model) the flow is constitutively stable for any De_κ. At any non-zero value of ξ increasing the value of De_κ (or the electric gradient, E_x) beyond a critical value produces a constitutively unstable flow. From Eq. (28), we find $|De_{\kappa,c}|$ only depends on ξ, when $\bar\kappa > 10$.

The variation of the dimensionless critical shear rate ($\lambda|\dot\gamma_c|$) with ε as a function of ξ is presented in Fig. 6 for $\xi = 0.001, 0.01$ and 0.1. The plot of critical shear rate versus ε shows a linear relationship for all ξ, as anticipated from Eq. (26). The critical shear rate gradually increases for $\xi = 0.01$ and 0.1, whereas, a steep rise with ε is observed as ξ decreases (cf. Fig. 6 with $\xi = 0.001$). In the limit, for $\xi = 0$ the curve is vertical, i.e., $\lambda|\dot\gamma|_c$ tends to infinity meaning stable flow.

Profiles of normal and shear stresses, drawn based on Eqs. (20) and (21), are shown in Fig. 7a and b as a function of y/H at $\bar\kappa = 10$ and 20 for different values of De_κ. The normal stress approaches zero for $y/H < 0.75$ and increases rapidly near the wall. At low De_κ the normal stress is almost zero near the wall for both $\bar\kappa = 10$ and 20. With increase in De_κ the normal stress increases gradually. The increase in normal stress is gradual for $\bar\kappa = 10$ compared to $\bar\kappa = 20$ where the rise is sudden in agreement with the corresponding variations of the velocity profile. A similar trend is observed for the shear stress profiles as seen in Fig. 7.
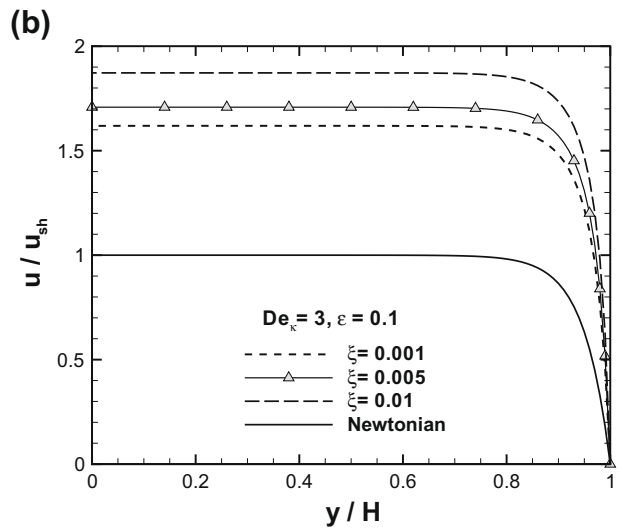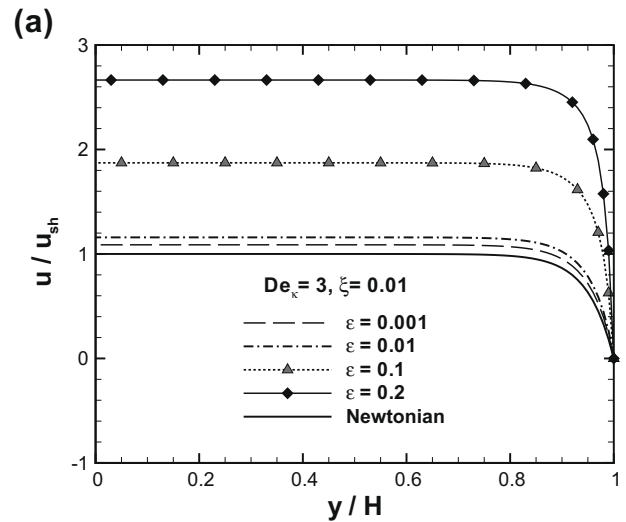

Fig. 4. Effect of (a) variation of ε at $De_\kappa = 3$ and $\xi = 0.01$ and (b) variation of ξ at $De_\kappa = 3$ and $\varepsilon = 0.1$ on the non-dimensional velocity profiles for the viscoelastic fluid flow in the microchannel under the influence of electro-osmotic forces. In all cases $\bar\kappa = 20$.
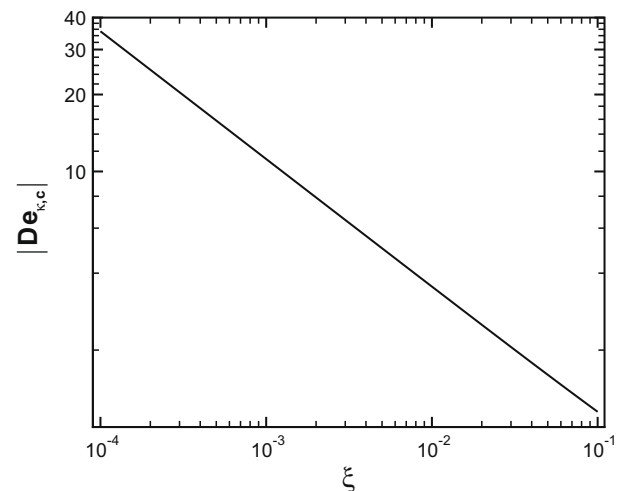

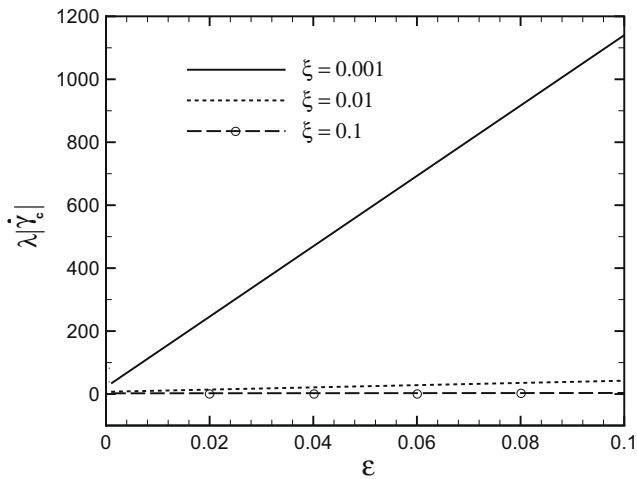**Fig. 5.** Variation of critical Deborah number ($|De_{\kappa,c}|$) with ξ.

Fig. 6. Variation of dimensionless critical shear rate $(\lambda|\dot{\gamma}_c|)$ with ε at $\xi = 0.001, 0.01$ and 0.1.
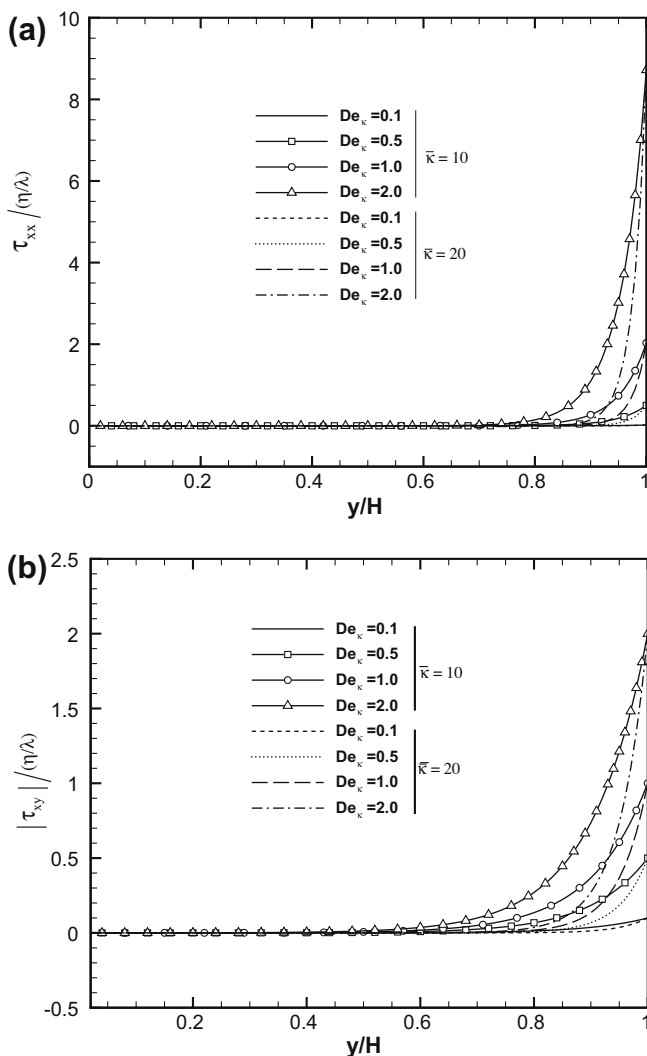

Fig. 7. (a) Normal stress (τ_{xx}) and (b) shear stress (τ_{xy}) as a function of y/H at different Deborah numbers (De_{κ}) for $\bar{\kappa} = 10$ and 20.

For the channel flow of viscoelastic fluids with electrokinetic forces, in the absence of Gordon–Schowalter derivative, Afonso

et al. [14,18] observed that the influences of ε and De_{κ} can be combined as a single dimensionless quantity, $\varepsilon De_{\kappa}^2$. In order to verify whether this also occurs here, we considered two sets of ϵ and De_{κ} so that $\varepsilon De_{\kappa}^2$ are equal to 0.1 and 0.4, keeping ξ constant and equal to 0.01. Results for the dimensionless transverse velocity profiles in the channel (not shown here) revealed that no such $\varepsilon De_{\kappa}^2$ scaling apply here compared to the sPTT model.

6. Conclusions

Analytical solutions in microchannels for the electro-osmotic flow of viscoelastic fluids obeying the full PTT model have been derived. The Gordon–Schowalter convected derivative has been used in this model which leads to non-zero second normal stress difference. Symmetric boundary conditions with equal zeta potentials at the walls were assumed. A nonlinear Poisson–Boltzmann equation governing the electrical double-layer field and a body force generated by the applied electrical potential field were included in the Navier–Stokes equations. Some of the important results can be summarised as follows:

- Comparison of the present result with the analytical solution, for the flow of Newtonian fluids, available in the literature is found to be consistent.
- Profiles of dimensionless velocities in the channel are invariant with De_{κ} below $De_{\kappa} = 0.1$.
- When the shear rate and Deborah number exceed a critical value a constitutive flow instability occurs for $\xi \neq 0$. Expressions for these critical values of shear rate and Deborah number are reported. The critical shear rate is found to be dependent of ε and ξ, whereas the critical Deborah number is only dependent on ξ for large $\bar{\kappa}$. The critical Deborah number increases with decrease in ξ tending to infinity as ξ tends to zero.
- Dimensionless normal and shear stresses are approximately zero near the centreline and rise rapidly near the channel walls. At low Deborah numbers both these quantities are almost negligible. At higher De_{κ} the values of these quantities rise rapidly with increasing microchannel height ratio.

References

[1] D. Burgreen, F.R. Nakache, J. Phys. Chem. 68 (1964) 1084–1091.
[2] C.L. Rice, R. Whitehead, J. Phys. Chem. 69 (1965) 4017–4024.
[3] P. Dutta, A. Beskok, Anal. Chem. 73 (2001) 1979–1986.
[4] S. Arulanandam, D. Li, Colloids Surf., A 161 (2000) 29–102.
[5] C. Wang, T. Wong, C. Yang, K. Ooi, Int. J. Heat Mass Transfer 50 (2007) 3115–3121.
[6] X. Wang, B. Chen, J. Wu, Phys. Fluids 19 (12) (2007) 127101.
[7] A.Q. Zade, M.T. Manzari, S.K. Hannani, Int. J. Heat Mass Transfer 50 (5–6) (2007) 1087–1096.
[8] S. Qian, H.H. Bau, Anal. Chem. 74 (15) (2002) 3616–3625.
[9] D.N. Petsev, G.P. Lopez, J. Colloid Interface Sci. 294 (2) (2006) 492–498.
[10] S. Qian, H.H. Bau, Appl. Math. Modell. 29 (8) (2005) 726–753.
[11] S. Das, S. Chakraborty, Anal. Chim. Acta 559 (2006) 15–24.
[12] S. Chakraborty, Anal. Chim. Acta 605 (2007) 175–184.
[13] M.L. Olivares, L.V. Candiotti, C.L.A. Berli, Electrophoresis 30 (2009) 921–929.
[14] A.M. Afonso, M.A. Alves, F.T. Pinho, J. Non-Newtonian Fluid Mech. 159 (2009) 50–63.
[15] N. Phan-Thien, R.I. Tanner, J. Non-Newtonian Fluid Mech. 2 (1977) 353–365.
[16] N. Phan-Thien, J. Rheol. 22 (1978) 259.

[17] R.B. Bird, P.J. Dotson, N.L. Johnson, J. Non-Newtonian Fluid Mech. 7 (1980) 213–235.

[18] A.M. Afonso, M.A. Alves, F.T. Pinho, J. Eng. Math., submitted for publication.

[19] J.J. Sousa, A.M. Afonso, F.T. Pinho, M.A. Alves, Effect of the skimming-layer on the electro-osmotic Poiseuille flows of viscoelastic fluids, III Conferencia Nacional em Mecanica de Fluidos, Termodinamica e Energia, Instituto Politecnico de Braganca, 17–18th September, Paper No. 10.

[20] D.A. Boy, B.D. Storey, Phys. Rev. E: Stat., Nonlinear, Soft Matter Phys. 76 (2) (2007) 026304.

[21] H. Lin, B.D. Storey, M.H. Oddy, C. Chen, J.G. Santiago, Phys. Fluids. 16 (2004) 1922.

[22] M.A. Alves, F.T. Pinho, P.J. Oliveira, J. Non-Newtonian Fluid Mech. 101 (2001) 55–76.

[23] P. Español, X.F. Yuan, R.C. Ball, J. Non-Newtonian Fluid Mech. 65 (1996) 93–109.

[24] G.C. Georgiou, D.V. Vlassopoulos, J. Non-Newtonian Fluid Mech. 75 (1998) 77–97.

[25] R.G. Larson, Constitutive Equations for Polymer Melts and Solutions, Butterworths, Boston, 1998.

[26] H. Bruss, Theoretical Microfluidics, Oxford Master Series in Condensed Matter Physics, Oxford University Press, Oxford, UK, 2008.

[27] R.F. Probstein, Physicochemical Hydrodynamics: An Introduction, second ed., Wiley Interscience, Hoboken, New Jersey, USA, 2003.